Journal of Applied Mechanics and Technical Physics, Vol. 42, No. 3, pp. 420–426, 2001

NUMERICAL SIMULATION OF HYPERSONIC FLOW AROUND A SHARP CONE

T. V. Poplavskaya and S. G. Mironov

UDC 532.526

A hypersonic viscous flow in the shock layer near sharp cones is considered. The profiles of density and velocity, the slopes of the shock wave, and the pressures and heat fluxes calculated on the basis of the full viscous shock layer equations are compared with available experimental and theoretical data.

Because of the computational difficulties in mathematical simulation of three-dimensional problems of a supersonic viscous flow around bodies within the framework of the full Navier–Stokes equations, the model of the full viscous shock layer (FVSL) has gained wide application. This model is an intermediate asymptotic approximation between the boundary-layer equations and the full Navier–Stokes equations [1, 2]. The FVSL model has been widely used recently to solve aerohydrodynamics and reentry problems. The authors of most papers consider the flow around smooth blunted cones [3–7]. A hypersonic flow around pointed bodies was studied within the framework of the viscid–inviscid interaction model [8–10] or the model of a thin shock layer [1, 11]. In [12–14], the FVSL model was used to calculate a hypersonic flow past a flat plate with a sharp edge.

The objective of the present work is to study theoretically the applicability of the FVSL model for calculation of a hypersonic shock layer on sharp cones and to study the influence of various parameters on the characteristics of such flows.

The flow in different regions in the vicinity of a sharp cone has a different character. There is a small region of free-molecular flow directly near the cone apex, then follows a continuum region of the merged layer, which is asymptotically transformed into the region of strong interaction. Further downstream, the regime of weak interaction is observed, where the inviscid flow plays an important role [15]. The spectrum of flow regimes on the cone is the same as on the flat plate; however, as is shown in [15, 16], the axisymmetric geometry of the cone changes the flow pattern: the shock wave (SW) approaches the cone surface (as compared to planar flows on the flat plate and on the wedge), and the boundary-layer thickness decreases. This increases the region of the merged layer and weakens the SW.

As in the two-dimensional case, the boundary of the merged layer and the region of strong interaction is determined by the rarefaction parameter $V = \mathrm{M}_\infty\sqrt{C}/\sqrt{\mathrm{Re}_x}$ (M_∞ is the free-stream Mach number, C is the Chapman–Rubezin constant, and Re_x is the local Reynolds number based on the free-stream parameters), which is maximum near the cone apex and decreases downstream. For a planar flow on a flat plate, the upper boundary of applicability of the FVSL model is the value $V = 0.1$–0.15. From the experimental results of [16], it follows that the length of the merged layer on sharp cones decreases with increasing cone half-angle; therefore, the FVSL calculations should start from greater values of the rarefaction parameter V: $V = 0.16$, 00.18, and 0.21 for a cone with a half-angles of 5°, 10°, and 15°, respectively.

Formulation of the Problem. We consider an axisymmetric hypersonic flow around a sharp cone. In the coordinate system attached to the body surface, the FVSL equations have the following form in dimensionless variables:

$$\frac{\partial}{\partial x}(r\rho u) + \frac{\partial}{\partial y}(r\rho v) = 0, \qquad \rho u\frac{\partial u}{\partial x} + \rho v\frac{\partial u}{\partial y} - \frac{1}{r\,\mathrm{Re}_L}\frac{\partial}{\partial y}\Big(r\mu\frac{\partial u}{\partial y}\Big) + \frac{\partial P}{\partial x} = 0,$$

$$\rho u\frac{\partial v}{\partial x} + \rho v\frac{\partial v}{\partial y} - \frac{4}{3}\frac{1}{r\,\mathrm{Re}_L}\frac{\partial}{\partial y}\Big(r\mu\frac{\partial v}{\partial y}\Big) + \frac{\partial P}{\partial y} = 0, \tag{1}$$

Institute of Theoretical and Applied Mechanics, Siberian Division, Russian Academy of Sciences, Novosibirsk 630090. Translated from Prikladnaya Mekhanika i Tekhnicheskaya Fizika, Vol. 42, No. 3, pp. 43–50, May–June, 2001. Original article submitted October 30, 2000; revision submitted December 25, 2000.

 0021-8944/01/4203-0420 $25.00

$$c_p\rho u\,\frac{\partial T}{\partial x}+c_p\rho v\,\frac{\partial T}{\partial y}-\frac{1}{r\,\mathrm{Re}_L\,\mathrm{Pr}}\,\frac{\partial}{\partial y}\Big(rk\,\frac{\partial T}{\partial y}\Big)-\frac{1}{\mathrm{Re}_L}\,(\gamma-1)\mathrm{M}_\infty^2\mu\Big(\frac{\partial u}{\partial y}\Big)^2$$

$$-(\gamma-1)\mathrm{M}_\infty^2\Big(u\,\frac{\partial P}{\partial x}+v\,\frac{\partial P}{\partial y}\Big)=0,\qquad P=\frac{1}{\gamma\,\mathrm{M}_\infty^2}\,\rho T.$$

Here the x and y axes are directed along the cone generatrix and perpendicular to it, $r=r_w+y\cos\theta$ is the distance from a point to the axis of symmetry, r_w is the distance from the body contour to the axis of symmetry, θ is the cone half-angle, P, ρ, μ, k, and T are the pressure, density, viscosity, thermal conductivity, and temperature, respectively, $\mathrm{Pr}=\mu_\infty c_{p\infty}/k_\infty$ is the Prandtl number, and $\mathrm{Re}_L=\rho_\infty U_\infty L/\mu_\infty$ is the Reynolds number based on the free-stream parameters and the model length L measured along the cone axis. The velocity components are normalized to the free-stream velocity U_∞, the pressure is related to the doubled dynamic pressure $\rho_\infty U_\infty^2$, the viscosity μ, thermal conductivity k, specific heat capacity c_p, density, and temperature are normalized to their free-stream values, and the coordinates x and y to the model length L.

The shock wave is assumed to be thin, and the generalized Rankine–Hugoniot conditions are set on it [17]:

$$u_s=\cos(\beta-\theta)[\cos\beta+k_s\tan(\beta-\theta)\sin\beta]-\frac{\mu_s\cos^3(\beta-\theta)[1-\tan^2(\beta-\theta)]}{\mathrm{Re}_L\sin(\beta+\alpha)}\,\frac{\partial u}{\partial y},$$

$$v_s=u_s\tan(\beta-\theta)-k_s\,\frac{\sin\beta}{\cos(\beta-\theta)},$$

$$P_s=\frac{1}{\gamma\mathrm{M}_\infty^2}+(1-k_s)\sin^2\beta-\frac{2\mu_s\sin(\beta-\theta)\cos(\beta-\theta)}{\mathrm{Re}_L}\,\frac{\partial u}{\partial y},\tag{2}$$

$$H_s=1+\frac{\gamma-1}{2}\,\mathrm{M}_\infty^2-\frac{\cos(\beta-\theta)}{\sigma_s\,\mathrm{Re}_L\,\sin\beta}\Big[\frac{\partial H}{\partial y}-\frac{1-\mathrm{Pr}}{2}\,(\gamma-1)\,\mathrm{M}_\infty^2\,\frac{\partial}{\partial y}\,(u^2)\Big],$$

$$k_s=\frac{1}{\rho_s},\qquad \sigma_s=\frac{\mathrm{Pr}}{\mu_s}.$$

Here β is the angle of SW inclination counted from the axis of symmetry of the cone, γ is the ratio of specific heats in the free stream, and H is the total specific enthalpy; the subscripts "∞" and s correspond to the free-stream parameters and the flow parameters behind the shock wave, respectively. To determine the SW shape y_s, we used the integral condition of flow-rate conservation in the transition through the SW:

$$(r+y_s\cos\theta)^2=2\int\limits_0^{y_s}\rho ur\cos\theta\,dy.\tag{3}$$

The boundary conditions on the cone were the slip conditions and the temperature jump [12–14, 18, 19].

To solve system (1), it is necessary to set the initial conditions for a certain $x=x_0$. As noted above, the FVSL calculations start from the boundary of the merged layer and strong interaction regions. From analysis of the experimental data of [15, 16, 20], it follows that the boundary layer near this interface fills almost the entire space between the body and the SW. Therefore, it is assumed that the flow is described by the equations of an axisymmetric boundary layer up to the cross section $x=x_0$, and the SW between the cone apex and the cross section $x=x_0$ has a constant slope. The initial conditions are determined in the same manner as in the problem for a flat plate [19]. For $x=x_0$, the system of FVSL equations (1) reduces to ordinary differential equations with the use of transformation of coordinates $\xi=x$ and $\eta=y\sqrt{\mathrm{Re}_L}/\sqrt{x}$, which is typical of boundary-layer flows in the case of a uniform external flow:

$$\frac{dJ}{d\eta}+\frac{1}{2}\,r\rho u=0,\quad J=r\sqrt{\xi}\,\rho v-0.5r\rho u\eta,\quad J\,\frac{du}{d\eta}-\frac{d}{d\eta}\Big(r\mu\,\frac{du}{d\eta}\Big)=0,\quad \frac{dP}{d\eta}=0,$$

$$c_pJ\,\frac{dT}{d\eta}-\frac{1}{\mathrm{Pr}}\,\frac{d}{d\eta}\Big(rk\,\frac{dT}{d\eta}\Big)-(\gamma-1)\,\mathrm{M}_\infty^2\mu r\Big(\frac{du}{d\eta}\Big)^2=0,\quad P=\frac{1}{\gamma\,\mathrm{M}_\infty^2}\,\rho T.\tag{4}$$

System (4) is solved under the following boundary conditions: for $\eta=0$, the quantities $J=0$, u, and T are determined from the slip conditions and temperature jump [19]; for $\eta=\eta_s$, we have $u=u_s$, $v=v_s$, $T=T_s$, and $\rho=\rho_s$. Here η_s is the SW position found from the mass-balance equation in the shock layer.

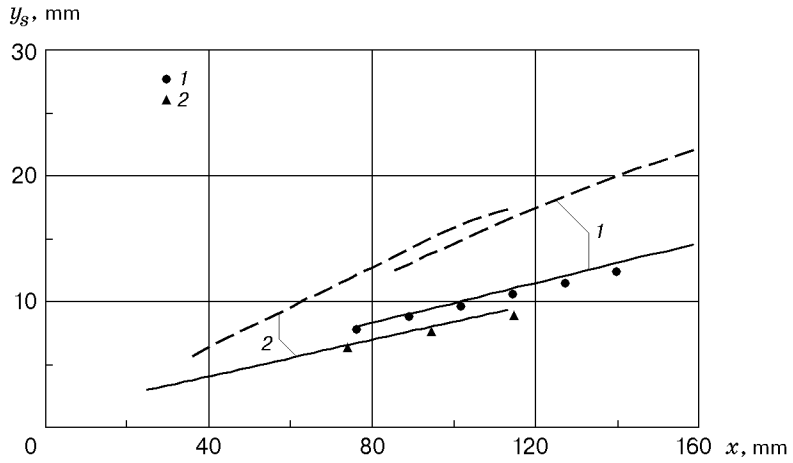

Fig. 1. SW position on the cone: the solid and dashed curves show the results of FVSL calculations for a cone and a flat plate, respectively; the points refer to experimental data for $M_\infty = 23.8$, $Re_L = 4.55 \cdot 10^4$, $T_0 = 2700$ K, $T_w = 300$ K, and $\theta = 5^\circ$ [16] (points 1) and $M_\infty = 21$, $Re_L = 6.78 \cdot 10^4$, $T_0 = 1150$ K, $T_w = 320$ K, and $\theta = 10^\circ$ [20] (points 2).

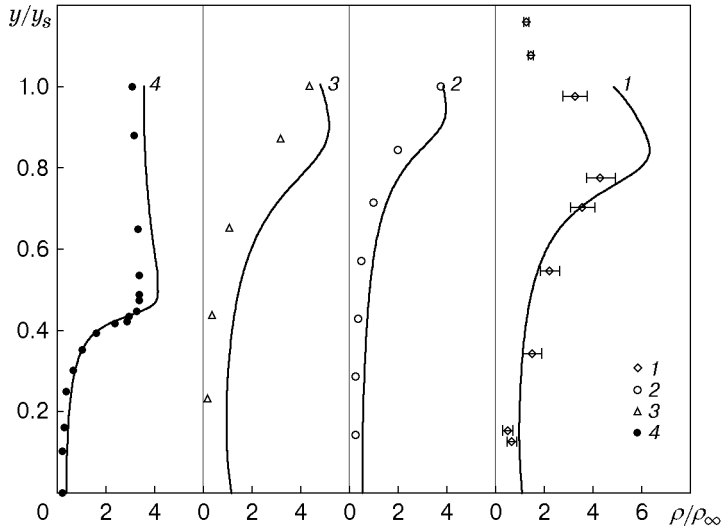

Fig. 2. Calculated (solid curves) and experimental (points) densities for $M_\infty = 21$, $Re_L = 6.78 \cdot 10^4$, $T_0 = 1150$ K, $T_w = 320$ K, and $\theta = 10^\circ$ [20] (points 1), $M_\infty = 25$, $Re_L = 1.05 \cdot 10^5$, $T_0 = 1850$ K, $T_w = 300$ K, and $\theta = 5^\circ$ [23] (point 2), $M_\infty = 24.5$, $Re_L = 3.6 \cdot 10^4$, $T_0 = 2000$ K, $T_w = 294$ K, and $\theta = 10^\circ$ [15] (point 3), and $M_\infty = 16.4$, $Re_L = 3.15 \cdot 10^5$, $T_0 = 297$ K, $T_w = 300$ K, and $\theta = 10^\circ$ [22] (point 4).

Algorithm of the Solution and Difference Scheme. The FVSL equations are solved using the following algorithm. First, ordinary differential equations (4) are solved in the region near the cone apex. The resultant profiles u_{ini}, v_{ini}, T_{ini}, P_{ini}, and ρ_{ini} are set as the initial conditions. Then the FVSL equations are solved by the marching method with respect to the x coordinate. Nonlinearity of system (1) requires the use of an iterative approach, which allows one to reduce the problem within one iteration to a sequential solution of difference boundary-value problems approximating system (1) by the shock-capturing method. The iterative process in each cross section is continued until the condition of flow-rate conservation in the transition through the SW (3) is fulfilled.

The solution of the problem yields the velocity, temperature, density, and pressure within the entire shock layer. On the cone surface, we calculate the friction coefficient $C_f = (\mu\, \partial u/\partial y)\Big|_{y=0} / (\rho_\infty U_\infty^2/2)$ and the heat-transfer coefficient $\text{St} = (k\, \partial T/\partial y + u\mu\, \partial u/\partial y)\Big|_{y=0} / [\rho_\infty U_\infty (H_\infty - H_w)]$ (Stanton number).

Since the FVSL equations include all terms of compressible boundary-layer equations, they were solved using a two-layer implicit difference scheme with second-order weights of accuracy in both directions, which was

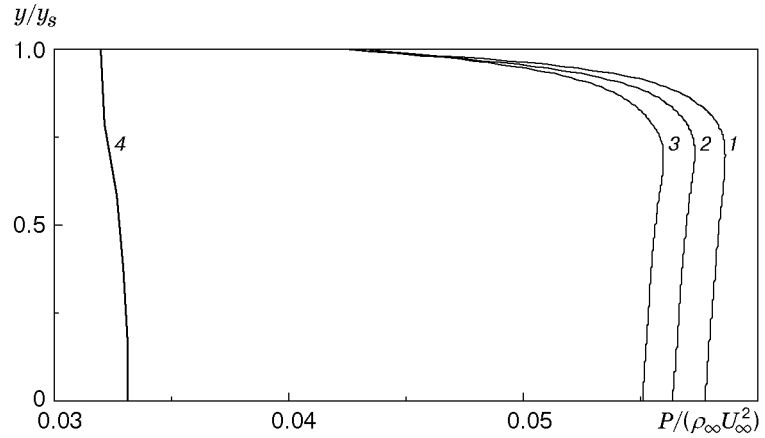

Fig. 3. Pressure distribution across the shock layer for $M_\infty = 21$, $Re_L = 6.78 \cdot 10^4$, $T_0 = 1150$ K, $T_w = 320$ K, and $\theta = 10°$: curves 1–3 refer to FVSL calculations for $x = 0.6$ (1), 0.8 (2), and 1 (3); curve 4 shows the calculation by the inviscid theory.

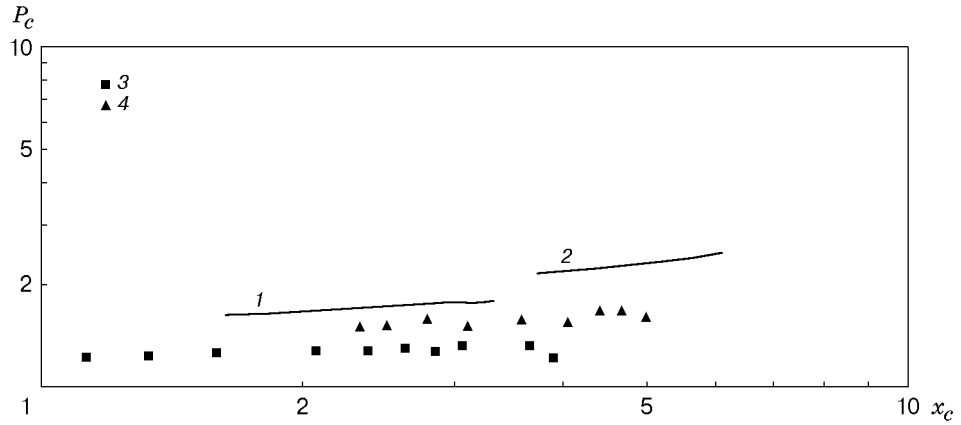

Fig. 4. Pressure distribution on the cone surface: the solid curves and points refer to the FVSL calculations and experimental data of [24], respectively, for $M_\infty = 15$, $Re_L = 8.1 \cdot 10^4$, $T_0 = 4000$ K, $T_w = 320$ K, and $\theta = 9°$ (curve 1 and points 3), $M_\infty = 15$, $Re_L = 6.4 \cdot 10^4$, $T_0 = 4000$ K, $T_w = 320$ K, and $\theta = 6.3°$ (curve 2), and $M_\infty = 15$–20, $Re_L = 6.4 \cdot 10^4$, $T_w/T_0 = 0.08$, and $\theta = 6.3°$ (points 4).

previously used in solving the boundary-layer equations [21]. FVSL calculations were performed on a difference grid with 200 points along the normal; the step along the x coordinate was chosen equal to 0.0001. A twofold increase in the number of grid points in both directions changed the solution by less than 2%. The Prandtl number was 0.7, $\gamma = 1.4$, and the viscosity was approximated by the Sutherland function.

Calculation Results. The results of solving the FVSL equations on the cone were compared with experimental data obtained at the Institute of Theoretical and Applied Mechanics of the Siberian Division of the Russian Academy of Sciences and with other available results.

Figure 1 shows a comparison of the calculated stand-off distance of the shock wave with the experimental data of [16, 20]. The results of the FVSL model for a sharp cone are shown by the solid curves. The difference in numerical and experimental values of the SW position is less than 10%. The dashed curves correspond to the FVSL calculations for a flat plate at angles of attack equal to cone half-angles 5 and 10°. In the case of a cone, due to its axisymmetric geometry, the SW approaches the body surface, and the boundary-layer thickness decreases.

The calculated and experimental profiles of density are plotted in Fig. 2. The density profiles 1 and 2 were measured by the method of electron-beam fluorescence; profiles 3 and 4 were recalculated from the measured values of pressure and temperature. The density profile 1 was measured in the wake flow behind the cone at a distance of $0.8D$ from the cone base (D is the cone-base diameter). It is assumed that the density profile in the wake at a distance of one diameter from the cone base still retains the distribution typical of the shock layer in the end cross section of the cone. If the measurements are performed in the absence of the surface in the flow, the method of electron-beam fluorescence has a better accuracy.

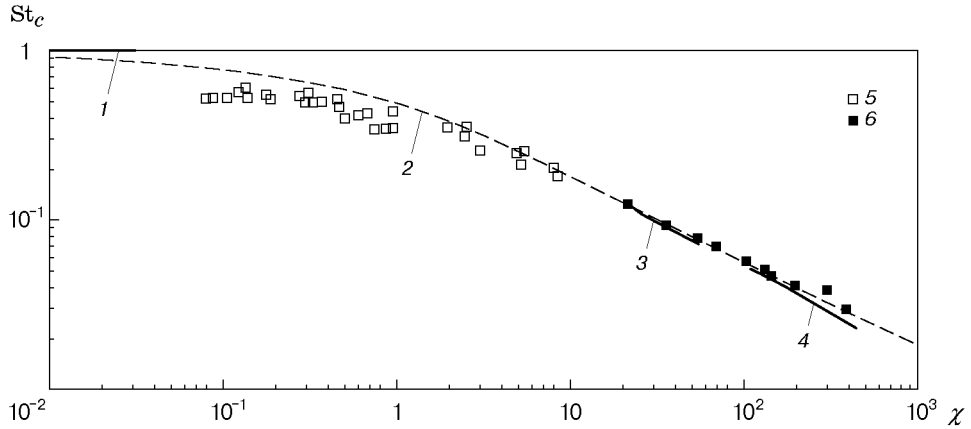

Fig. 5. Stanton number distribution on the cone surface: 1) free-molecular limit [24]; 2) theory of a thin viscous shock layer ($\theta = 10^\circ$) [1]; 3) present calculations ($M_\infty = 19$–24, $Re_L = 1.73 \cdot 10^4$, $T_0 = 4000$ K, $T_w = 320$ K, and $\theta = 10^\circ$); 4) present calculations ($M_\infty = 15$, $Re_L = 8.1 \cdot 10^4$, $T_0 = 4000$ K, $T_w = 320$ K, and $\theta = 9^\circ$); 5) $M_\infty = 19$–24, $Re_L = 6.48 \cdot 10^2$–$1.73 \cdot 10^4$, $T_w/T_0 = 0.08$, and $\theta = 10^\circ$ [24]; 6) $M_\infty = 15$, $Re_L = 8.1 \cdot 10^4$, $T_0 = 4000$ K, $T_w = 320$ K, and $\theta = 9^\circ$ [24].

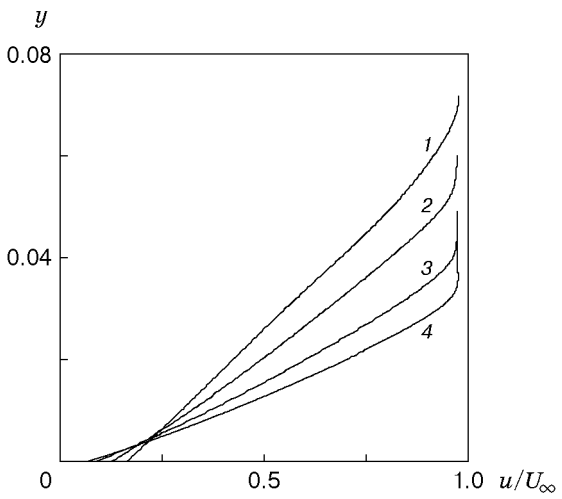

Fig. 6

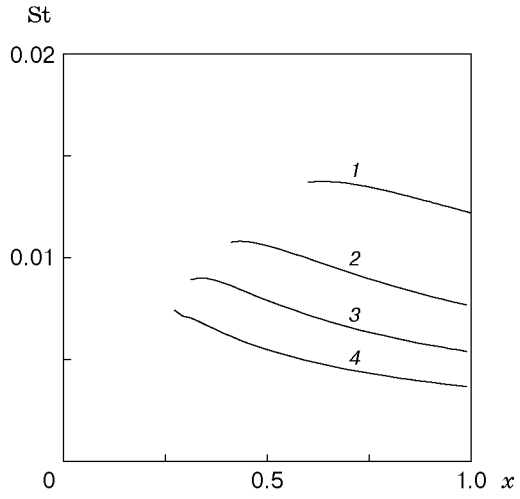

Fig. 7

Fig. 6. Velocity distribution over the transverse coordinate for $M_\infty = 21$, $T_0 = 1150$ K, $T_w = 320$ K, $\theta = 10^\circ$, and $Re_L = 3 \cdot 10^4$ (1), $6.78 \cdot 10^4$ (2), $1.2 \cdot 10^5$ (3), and $2.4 \cdot 10^5$ (4).

Fig. 7. Stanton number distribution over the longitudinal coordinate for $M_\infty = 21$, $T_0 = 1150$ K, $T_w = 320$ K, and $\theta = 10^\circ$ (notation the same as in Fig. 6).

FVSL calculations showed that the density maximum is not located on the SW as in the case of a flat plate; it is located lower, in the inviscid part of the shock layer, which is confirmed by the experimental data of [20]. This is, apparently, related to the axisymmetric geometry of the cone, which leads to SW attenuation. Figure 3 shows the pressure as a function of the coordinate normal to the surface, which was calculated by the FVSL model in the cross sections $x = 0.6$, 0.8, and 1.0 (curves 1–3, respectively). Curve 4 is the pressure distribution obtained by the inviscid theory for the same Mach number ($M_\infty = 21$). In both cases, the pressure minimum is located on the SW. In the flow past a flat plate, the pressure maximum is on the SW [19]; therefore, the position of the density maximum coincides with the SW position. On the cone, the pressure reaches a maximum in the inviscid region of the shock layer located behind the SW; therefore, the density maximum is reached at a certain distance from the SW.

Figure 4 shows the pressure $P_c = (P/P_\infty)/(\gamma \mathrm{M}_\infty \sin^2\theta)$ measured on the cone surface as a function of the parameter $x_c = \mathrm{M}_\infty\sqrt{C}/(\mathrm{Re}_x \sin^2\theta)$ [24]. The calculated data obtained by the FVSL model (curves 1 and 2) for the same parameters as in the experiment are higher than the experimental data (the difference is less than 25%).

Figure 5 shows the calculated and measured values of the Stanton number $\mathrm{St}_c = \mathrm{St}\,(1 - T_w/T_0)/\sin\theta$ (T_0 is the stagnation temperature) versus the parameter $\chi = \mathrm{Re}_x/(\mathrm{M}_\infty^2 C\gamma\cos\theta)$ [24]. The same figure shows the results of the present calculations (curves 3 and 4). The Stanton numbers calculated by the FVSL model are in good agreement with experimental data and with calculations by the theory of a thin viscous shock layer [1].

It should be noted that the calculation results depend significantly on the Reynolds number. Its effect on velocity profiles and heat fluxes is shown in Figs. 6 and 7. With increasing Re_L, the SW stand-off distance decreases, the velocity profiles (Fig. 6) "press" against the cone surface, and the values of St (Fig. 7) decrease monotonically in all x sections. Note that a twofold decrease in Re_L leads to a 30% increase in the Stanton number. In the present work, the Reynolds number was calculated from the free-stream parameters as follows. The density and velocity were found from isentropic formulas taking into account vibrational degrees of freedom. The viscosity was determined by the linear law for temperatures lower than 120 K and by the Sutherland law for temperatures higher than 120 K. Probably, this method of Reynolds number calculation differs from that used in [24]; therefore, the present calculations differ from the experimental results.

Thus, an algorithm for the numerical solution of the FVSL equations for a sharp cone at zero angle of attack was developed. All characteristics of the flow for various Mach and Reynolds numbers were calculated. Satisfactory agreement of numerical and experimental data was obtained.

The authors are grateful to A. A. Maslov and V. N. Vetlutsky for useful discussions and valuable comments.

This work was supported by the Russian Foundation for Fundamental Research (Grant No. 98-01-00735).

REFERENCES

1. H. K. Cheng, J. Gordon Hall, T. C. Golian, and A. Hertzberg, "Boundary-layer displacement and leading-edge bluntness effects in high-temperature hypersonic flow," *J. Aerospace Sci.*, **28**, No. 5, 353–381 (1961).
2. R. T. Davis, "Numerical solution of the hypersonic viscous shock-layer-equations," *AIAA J.*, **8**, No. 5, 843–851 (1970).
3. S. A. Vasil'evskii, G. A. Tirskii, and S. V. Utyuzhnikov, "Numerical method for solving the viscous shock layer equations," *Zh. Vychisl. Mat. Mat. Fiz.*, **27**, No. 5, 741–750 (1987).
4. G. A. Tirskii and S. V. Utyuzhnikov, "Comparison of the models of a thin and full viscous shock layer in the problems of a supersonic viscous flow around blunted cones," *Prikl. Mat. Mekh.*, **53**, No. 6, 963–969 (1989).
5. R. T. Davis and S. G. Rubin, "Non-Navier–Stokes viscous flow computations," *Comput. Fluids*, **8**, No. 1, 101–131 (1980).
6. A. I. Borodin and S. V. Peigin, "Method of global iterations for solving three-dimensional equations of a viscous shock layer," *Teplofiz. Vys. Temp.*, **30**, No. 6, 1124–1129 (1992).
7. A. I. Borodin and S. V. Peigin, "Model of a parabolized viscous shock layer for studying a three-dimensional hypersonic viscous flow around bodies," *Teplofiz. Vys. Temp.*, **31**, No. 6, 925–933 (1993).
8. R. F. Probstein and E. Elliott, "The transverse curvature effect in compressible axially symmetric laminar-boundary-layer flow," *J. Aeronaut. Sci.*, No. 28, 208–224 (1956).
9. N. Yasuhara, "Axisymmetric viscous flow past very slender bodies of revolution," *J. Aeronaut. Sci.*, No. 29, 667–688 (1962).
10. K. Stewartson, "Viscous hypersonic flow past a slender cone," *Phys. Fluids*, No. 7, 667–675 (1964).
11. R. R. Eaton and P. C. Kaestner, "Viscous shock layer flow in the windward plane of cones at angle of attack," AIAA Paper No. 73-134 (1973).
12. A. A. Maslov, S. G. Mironov, T. V. Poplavskaya, et al., "Viscous shock layer on a plate in hypersonic flow," *Europ. J. Mech., B-Fluids*, **18**, No. 2, 213–226 (1999).
13. A. A. Maslov, S. G. Mironov, T. V. Poplavskaya, and V. N. Vetlutsky, "Effect of the angle of attack on the hypersonic flow past a flat plate," *Teplofiz. Vys. Temp.*, **36**, No. 5, 754–760 (1998).
14. A. A. Maslov, S. G. Mironov, T. V. Poplavskaya, et al., "Investigation of aerodynamic heating of a flat plate in a viscous hypersonic flow," *Teplofiz. Vys. Temp.*, **37**, No. 3, 415–419 (1999).
15. W. J. McCroskey, S. M. Bogdonoff, and A. P. Genchi, "Leading edge flow studies of sharp bodies in rarefied hypersonic flow," in: *Rarefied Gas Dynamics*, Vol. 2, Academic Press, New York–London (1967), pp. 1047–1066.

16. R. A. Feik, A. P. Genchi, and I. E. Vas, "A study of merging on cones," in: *Rarefied Gas Dynamics*, Vol. 1, Academic Press, New York–London (1969), pp. 493–500.
17. G. A. Tirskii, "Theory of hypersonic flow around planar and axisymmetric blunted bodies by a viscous, chemically reacting gas with injection," in: *Scientific Papers of the Institute of Mechanics at the Moscow State University* [in Russian], No. 39 (1975), pp. 5–39.
18. V. N. Vetlutsky, A. A. Maslov, S. G. Mironov, et al., "Hypersonic flow on a flat plate. Experimental results and numerical simulation," *Prikl. Mekh. Tekh. Fiz.*, **36**, No. 6, 60–67 (1995).
19. T. V. Poplavskaya and V. N. Vetlutsky, "Numerical study of a viscous shock layer on a plate," *Prikl. Mekh. Tekh. Fiz.*, **38**, No. 2, 91–100 (1997).
20. V. M. Aniskin and S. G. Mironov, "Experimental study of density fluctuations in a hypersonic laminar wake behind a cone," *Prikl. Mekh. Tekh. Fiz.*, **41**, No. 3, 111–117 (2000).
21. V. N. Vetlutsky and T. V. Poplavskaya, "Calculation of a laminar boundary layer on a flat triangular plate with supersonic leading edges," in: *Numerical Methods of Continuum Mechanics* [in Russian], Vol. 13, No. 1, Inst. of Theor. and Appl. Mech., Sib. Div., Acad. of Sci. of the USSR (1982), pp. 31–43.
22. I. E. Vas and J. G. Sierchio, "Downstream effects of bluntness in the merged flow regime," in: *Rarefied Gas Dynamics*, Academic Press, New York (1974), pp. 307–315.
23. C. W. Peterson, "An experimental study of laminar hypersonic blunt cone wakes," *Astronaut. Acta*, **15**, 67–76 (1969).
24. H. F. Waldron, "Viscous hypersonic flow over pointed cones at low Reynolds numbers," *AIAA J.*, **5**, No. 2, 208–218 (1967).